

Bridge the Gap Between Model-based and Model-free Human Reconstruction

Lixiang Lin
Zhe Jiang University
lxl@zju.edu.cn

Jianke Zhu
Zhe Jiang University
jkzhu@zju.edu.cn

Abstract

It is challenging to directly estimate the geometry of human from a single image due to the high diversity and complexity of body shapes with the various clothing styles. Most of model-based approaches are limited to predict the shape and pose of a minimally clothed body with over-smoothing surface. Although capturing the fine detailed geometries, the model-free methods are lack of the fixed mesh topology. To address these issues, we propose a novel topology-preserved human reconstruction approach by bridging the gap between model-based and model-free human reconstruction. We present an end-to-end neural network that simultaneously predicts the pixel-aligned implicit surface and the explicit mesh model built by graph convolutional neural network. Moreover, an extra graph convolutional neural network is employed to estimate the vertex offsets between the implicit surface and parametric mesh model. Finally, we suggest an efficient implicit registration method to refine the neural network output in implicit space. Experiments on DeepHuman dataset showed that our approach is effective.

1. Introduction

Human reconstruction has been studied for decades, which is essential to a large amount of real-world applications, including motion capture, digital entertainments, etc.

Generally, it is challenging to directly estimate the geometry of human from a single RGB image due to the high diversity and complexity of body shapes. Moreover, the sophisticated clothing styles often lead to the extra difficulties.

To tackle this critical problem, the statistical human models like SCAPE [3] and SMPL [15] are proposed to reduce the searching space through the parametric methods built by Principal Component Analysis (PCA) and blend skinning. Recently, the deep neural network-based methods [12, 13] try to estimate the model parameters from image without resorting to the time-consuming nonlinear optimization. Although having achieved the promising results, most of these approaches are still limited to capture



(a) SMPL fitting [12] (b) PIFu [26] (c) Our method

Figure 1. The model-based approach [12] tries to estimate the SMPL parameters, which mainly captures the shape and pose without the details like clothing. The model-free method [26] recovers the fine detailed body geometry while the reconstructed mesh does not have the predefined topology. Our proposed approach is able to directly estimate accurate body mesh with the fixed topology.

the shape and pose of a minimally clothed body with over-smoothing surface, which is lack of the capability to represent a human with usual clothing and details. In spite of some parametric clothing models [21, 14, 33], they may not generalize well in the real scenario. Furthermore, it is hard to directly estimate the highly non-linear SMPL model parameters through deep neural networks.

Instead of relying on the parametric models, the model-free approaches [29, 35] directly reconstruct the human body from single image, which enjoy the merits of recovering the fine detailed geometries. To this end, human body is either estimated by the occupancy of small voxels [29, 35] or implicitly represented by a function learned by deep neural network [26]. The main showstopper for these methods is that there is no commonly-shared topology for the reconstructed body geometries. Therefore, it is difficult to find the semantic correspondences between the reconstructed mesh and human body part in contrast to the model-based approaches. This further prevents them from animating the reconstructed body directly.

To address the above limitations, this paper proposes a novel topology-preserved human reconstruction approach by taking advantage of both model-based and model-free methods. As shown in Fig. 1, we aim to accurately reconstruct the triangulated body mesh with the same topology as

SMPL model. Specifically, we present an end-to-end neural network that simultaneously predicts the pixel-aligned implicit surface and the explicit mesh model built by graph convolutional neural network (GCN). Moreover, an extra graph convolutional neural network is employed to estimate the vertex offsets between the implicit surface and parametric mesh model. All the decoder branches share the same feature encoder that greatly reduces the computational cost for inference. Finally, we suggest an effective implicit registration stage to refine the neural network output, which is performed in implicit space without resorting to the computational intensive Chamfer distance.

In summary, the main contributions of this paper are: (1) an end-to-end neural network that reconstructs the fine detailed body mesh while retaining the fixed topology from a single image; (2) a graph convolutional network to recover human mesh model as well as bridge the gap between the pixel-aligned implicit surface and recovered mesh model; (3) an efficient implicit registration method to refine the predicted mesh; (4) empirical evaluations on DeepHuman dataset showing promising human reconstruction results.

The rest of this paper is organized as follows. Section 2 reviews previous methods. Section 3 proposes our novel approach to human reconstruction, and presents the network scheme. Section 4 describes the experimental results. Section 5 concludes the paper and suggests some future work.

2. Related Work

Recovering of 3D human body shapes from 2D images or videos is the fundamental problem in computer vision, which has already been extensively studied for decades. Generally, most of existing approaches can be roughly divided into two categories. The first is dependent on the parametric models, which formulates the human body reconstruction as a regression problem. On the other hand, model-free methods try to reconstruct detailed human geometry directly.

2.1. Model-based Human Reconstruction

Due to the high diversity and complexity of poses with various shapes, it is very challenging to build the human body models with the desired generalization capability. During past fifteen years, a surge of research efforts have been devoted to building the statistical human body models from 3D laser scans [3, 15, 11, 23]. Angelov et al. [3] present a pose deformation-based model that derives the nonrigid surface deformation as a function on the pose of the articulated skeleton. Loper et al. [15] build a skinned vertex-based model with the shape and pose parameters, in which the pose-dependent blend shapes are a linear function of the elements of the pose rotation matrices. This makes it easy to integrate the human body generation process into the deep neural network pipeline for

back propagation. Recently, graph convolutional network becomes more and more important in dealing with non-rigid shape like face [25], which requires fewer parameters and can achieve higher accuracy compared with the parametric models. Choi et al. [7] propose a graph convolutional network that recovers 3D human mesh from 2D human pose.

With the body shape models, human reconstruction is reduced to the parameter estimation problem, where the coefficients and joints transformation are directly predicted from the still image. The conventional methods [6, 32, 23] employ the nonlinear optimization solver to obtain the reasonable solution, which are usually computational intensive. Kanazawa et al. [12] propose an end-to-end framework to recover the human body shape and pose by estimating SMPL parameters using only 2D joints annotations with an adversarial loss. Kolotouros et al. [13] introduce a self-improving system which combines optimization and prediction methods. Most of these approaches only produce a naked human body, where the surfaces of clothing, hair, and other accessories are ignored.

To tackle the above problem, clothing is represented as an offset layer from the underlying body in [2, 1, 36, 24], which is able to change the pose and shape of the reconstruction using SMPL. Neophytou and Hilton [21] learn a layered garment model on top of SCAPE from dynamic sequences, however, it may not generalize well to novel poses. Yang et al. [33] train a neural network to regress a PCA-based representation of clothing. Moreover, Lahner et al. [14] learn a garment-specific pose-deformation model by regressing low-frequency PCA components and high frequency normal maps. Adam model [11] is clothed while the shape is very smooth and not pose-dependent. Recently, Ma et al. [17] present a generative 3D mesh model of clothed people, which is conditioned on both pose and clothing type. This enables the capability of drawing clothing samples to dress different body shapes in a variety of styles and poses. In contrast to these methods, our proposed approach does not require to build an extra parametric model for the dressing, which is able to handle the case without clothing as well.

2.2. Model-free Human Reconstruction

Model-free approaches try to directly estimate human body geometry like voxels or implicit surface from the still image without resorting to a prior model, which have much larger solution space to represent the fine details.

Varol et al. [29] suggest to learn a voxel representation of human body through the deep neural network, where the fine-scale details are often missing due to the high memory requirements of voxel representations. Zeng et al. [35] introduce a discretized volumetric representation to reconstruct the detailed human, which fuse the different scales of image features in order to recover the accurate surface

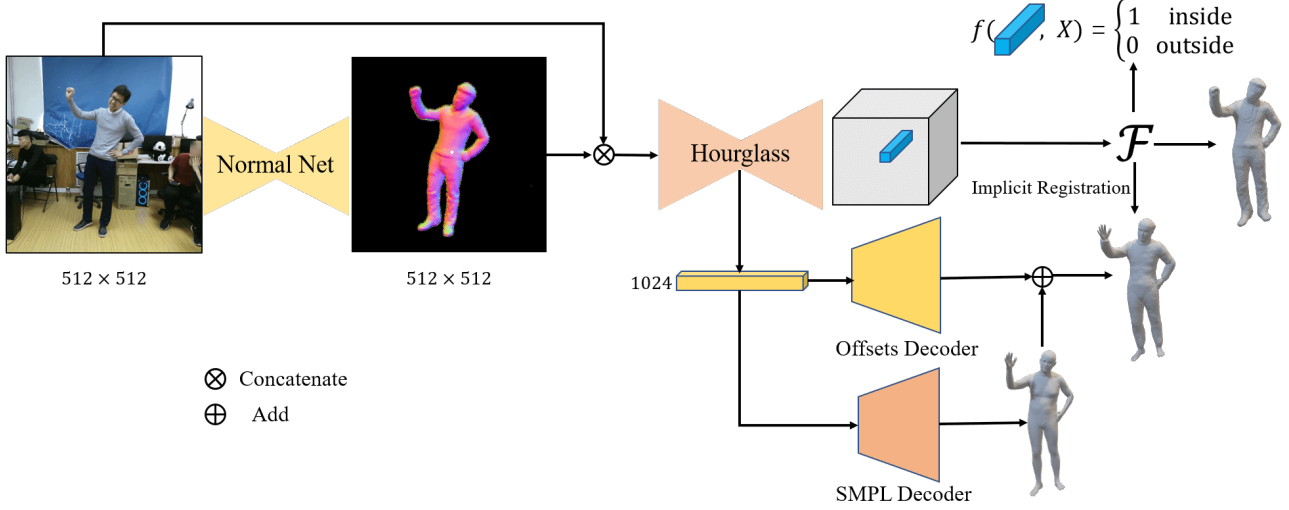


Figure 2. Overview of our proposed human reconstruction approach. We firstly concatenate the input image and estimated normal to feed the hourglass encoder. Then, a pixel-aligned implicit function predicts the occupancy, and two GCN decoders estimate the mesh model and offset to the implicit surface, respectively. Finally, the network inference result is refined through an effective implicit registration stage.

geometry. In spite of impressive results, the cubic memory requirement imposed by the discrete voxel representation prevents these methods from obtaining the high resolution reconstruction results. Instead of using the voxels, some approaches [8, 28] try to predict depth maps of human as output. Natsume et al. [20] present a multi-view inference method by synthesizing silhouette views from a single image. Although multi-view silhouettes are more memory efficient, the concave regions are difficult to infer as well as the consistently generated views.

Saito et al. [26] propose a memory efficient approach that represents the detailed human by a pixel-aligned implicit function. Instead of explicitly discretizing the output space into voxels, it regresses a function that determines the occupancy for any locations. With such implicit representation, the occupancy for the sampled 3D point can be computed on the fly, which greatly saves the memory. Later, Saito et al. [27] introduce a multi-level architecture for high-resolution 3D human reconstruction, where the coarse level focuses on the holistic reasoning and the fine level estimates the highly detailed geometry. Bhatnagar et al. [4] recover human model from the incomplete point cloud by combining implicit functions with parametric model, which is close to our proposed method. Instead of using scatted points, we directly perform reconstruction using image.

3. Methods

In this section, we present our proposed approach to human reconstruction from a single image. Firstly, we propose an end-to-end neural network that reconstructs the fine detailed body mesh while retaining the fixed topology. Secondly, we describe the model-free reconstruction using implicit surface loss. Thirdly, we introduce the graph convolu-

tional network approach to recovering human mesh model. Finally, we suggest to make use of another graph convolutional network to fill the gap between the pixel-aligned implicit surface and the recovered mesh model.

3.1. Overview

The model-based human reconstruction approach [12] enjoys the merit of the predefined mesh topology, which is able to preserve the body shape through the statistical models. On the other hand, the model-free method can recover the fine detailed geometry like wrinkles on the clothing. The key idea of our proposed approach is to take advantage of both representations. To this end, we aim to reconstruct the triangulated body mesh accurately while preserving the same topology as SMPL model. As illustrated in Fig. 2, we present an end-to-end deep neural network with a typical encoder-decoder structure.

In [27], the frontal normal map is predicted as a proxy for 3D geometry and extract features from normal maps for the sharper reconstructed results. Therefore, we firstly employ a pre-trained Pix2PixHD network [30] to obtain the frontal normal map, and then concatenate it with the original image as the input for the feature encoder. The Pix2PixHD network consists of nine residual blocks with four down-sampling layers, which is trained with the following loss:

$$\mathcal{L}_{\mathcal{N}} = \lambda_N \sum_{\{i,j\} \subset P} |n_{i,j} - n_{i,j}^*| + \lambda_m \sum_{\{i,j\} \not\subset P} |n_{i,j}| \quad (1)$$

where P denotes the index of the ground truth normal map that is valid. The first term is the regular L_1 loss. Due to the noisy environment, the second term is employed to remove the influence of background. We try to predict the frontal normal map of the person in the image, and set the values

of other places to 0. The weights of these two loss functions are $\lambda_N = 5$, $\lambda_m = 1$, respectively. We use Adam optimizer with the learning rate of 2×10^{-4} until convergence.

It is worthy of mentioning that we suggest to share the same feature encoder for all the decoder branches, which greatly reduces the computational cost during the inference. Moreover, a decoder branch is employed to predict the implicit surface function for the model-free human reconstruction, and another decoder branch is used to extract the explicit mesh surface using graph convolutional neural network trained on a large corpus. More importantly, we propose to train an extra graph convolutional neural network to fill the gap between the other two branches, which intends to reduce the registration error between the triangulated mesh and implicit surface.

From the above all, the proposed deep neural network minimizes the following loss function:

$$\mathcal{L} = \mathcal{L}_{\mathcal{I}} + \mathcal{L}_{\mathcal{M}} + \mathcal{L}_{\Delta} \quad (2)$$

where $\mathcal{L}_{\mathcal{I}}$ is the loss for implicit surface function estimation, and $\mathcal{L}_{\mathcal{M}}$ is the loss to recover the human mesh through GCN decoder. \mathcal{L}_{Δ} is the penalty for the detailed reconstruction, which bridges the gap between the model-free reconstruction and parametric mesh model. Finally, we suggest an implicit registration stage to further refine the results.

3.2. Implicit Reconstruction Loss $\mathcal{L}_{\mathcal{I}}$

Motivated by the model-free human reconstruction approach [26], we try to estimate the body surface through an implicit function $f(\cdot)$ that approximates the signed distance of zero level set. Instead of using the orthogonal projection with depth only in the conventional method [27], we suggest to take advantage of the full perspective projection, where the implicit surface shares the same coordinate space as SMPL mesh model. Specifically, a fully connected layer has the number of neurons (259,1024,512,256,128,1) with the skip connections at (3,4,5) layers, which is employed to predict the binary occupancy value for any given positions $X_i = (x_i, y_i, z_i) \in \mathbb{R}^3$ in the continuous 3D space:

$$f(\mathcal{F}_{\mathbf{x}_i}, X_i) = \begin{cases} 1, & \text{if } X_i \text{ is inside mesh surface} \\ 0, & \text{otherwise} \end{cases} \quad (3)$$

where $\mathcal{F}_{\mathbf{x}_i}$ denotes the deep features sampled at the location $\mathbf{x}_i = (u_i, v_i)$ in image space $\Omega \subset R^2$. The projection function $\pi : R^3 \rightarrow \Omega$ of conventional pinhole-camera model is defined as below:

$$\mathbf{x}_i = \pi(X_i) = \begin{pmatrix} K_u \frac{x_i}{z_i} + c_u \\ K_v \frac{y_i}{z_i} + c_v \end{pmatrix}, \quad (4)$$

where (K_u, K_v) is the focal length, and (c_u, c_v) is the principal point. To facilitate the effective reconstruction, we

employ the stacked hourglass network [22] with four stacks as the backbone to extract deep features $\mathcal{F}_{\mathbf{x}_i}$.

Given the the ground truth occupancy $y(X_i)$ at point X_i , we employ the extended Binary Cross Entropy (BCE) loss [35] to supervise our proposed implicit surface representation layer. Therefore, the implicit reconstruction loss $\mathcal{L}_{\mathcal{I}}$ can be derived as follows:

$$\mathcal{L}_{\mathcal{I}} = \sum_{X_i \in \mathcal{S}} \eta y(X_i) \log f(X_i) + (1 - \eta)(1 - y(X_i)) \log(1 - f(X_i)) \quad (5)$$

where \mathcal{S} is the set of the sampled points. η represents the ratio of points outside surface in \mathcal{S} , which is computed from the sampling results. A mixture sampling strategy is used to select the points for the implicit reconstruction loss computation. In our experiment, the sampled points are composed of the uniform sampling and importance sampling with the standard deviations of 0.2 and the ratio of 8 : 1. For the ground truth points and their occupancy, we make use of the human performance capture in DeepHuman dataset [35], which is based on the RGB-D optimization [34].

3.3. Mesh Recovery Loss $\mathcal{L}_{\mathcal{M}}$

The model-based human reconstruction has the merit of the watertight mesh representation with the data-driven priors, where the generative SMPL [15] model is widely used. It is based on an artist-created mesh with 6890 vertices and 24 joints, which is parameterized by the latent shape coefficients and poses through the shape-dependent deformations and pose-dependent deformations. Although formulating the pose blend shapes as a linear function of the rotation matrices for each part, the whole procedure of mesh generation is still highly nonlinear. Therefore, it is challenging to directly regress them from a single image directly.

To deal with this problem, we suggest to make use of a graph convolutional network-based autoencoder to capture human body shapes, which shares the same mesh topology as SMPL model without the blend skinning. In this paper, we employ the same loss function described in [7] to train our proposed GCN autoencoder and regress the latent coefficients from the extracted feature. For each vertex V_i in \mathcal{M} with the target V_i^* , the mesh recovery loss $\mathcal{L}_{\mathcal{M}}$ is defined as below:

$$\mathcal{L}_{\mathcal{M}} = \lambda_v \sum_{V_i \in \mathcal{M}} \|V_i - V_i^*\|_1 + \lambda_e \mathcal{L}_{edge} + \lambda_n \mathcal{L}_{normal} \quad (6)$$

where the first term denotes the per vertices L_1 fitting loss, and the last two terms regularizes the mesh deformations on edges and normals, respectively. Let \mathcal{T} represent a facet in \mathcal{M} and (i, j) are the vertex indices in \mathcal{T} , the edge length loss is derived as follows:

$$\mathcal{L}_{edge} = \sum_{\mathcal{T} \in \mathcal{M}} \sum_{\{i, j\} \in \mathcal{T}} \left| \|V_i - V_j\|_2 - \|V_i^* - V_j^*\|_2 \right| \quad (7)$$

Given the target normal n_f^* for each facet \mathcal{T} , the normal consistency loss is defined as in [7]:

$$\mathcal{L}_{normal} = \sum_{\mathcal{T} \in \mathcal{M}} \sum_{\{i,j\} \in \mathcal{T}} \left| \left\langle \frac{V_i - V_j}{\|V_i - V_j\|_2}, n_f^* \right\rangle \right| \quad (8)$$

The weights are $\lambda_v = 5$, $\lambda_e = 40$, and $\lambda_n = 0.5$.

As in [17], our proposed autoencoder consists of an encoder-decoder pair built by graph convolutional network. To embed the input data into the latent space, the encoder is made of eight Chebyshev Residual Blocks with Chebyshev polynomial of order two, a Chebyshev convolution with order one and a fully connected layer. Each graph convolution layer is followed by a Leaky ReLU [18]. On the other hand, the architecture of decoder is similar to the encoder except having the group normalization [31] before Leaky ReLU. For the detailed network structure, please refer to the supplementary materials. To effectively capture the various body shapes and poses, we train this autoencoder on AMASS [19] and Human3.6M [10] datasets. In contrast to COMA [25] reconstructing the smoothing facial meshes, our proposed method has to tackle the critical challenges of body articulations and blend skinning, which are usually highly nonlinear.

Once GCN autoencoder is trained, we freeze the model parameters of decoder and integrate it into our proposed human reconstruction framework to facilitate the mesh model generation. Moreover, we formulate the model-based reconstruction as the GCN latent embedding estimation problem. By adding a linear layer after the feature map, we employ an average pooling to downsample the feature map and a fully connected layer that has the number of neurons of (1024, 1024, 1024, 64) to adapt the number of features. We employ $\mathcal{L}_{\mathcal{M}}$ to supervise the training process.

3.4. Detailed Reconstruction Loss \mathcal{L}_{Δ}

To enable our proposed approach to capture the details of human body with the fixed topology, we suggest to take advantage of another GCN decoder predicting the offset between the pixel-aligned implicit surface and the recovered GCN mesh. Moreover, the GCN decoder for the detailed reconstruction shares the same network structure with the one for the mesh model estimation while its weights are not fixed during training. Let \mathcal{M} denote the mesh recovered by GCN decoder, and \mathcal{M}^* represents the target mesh captured by RGB-D optimization. The objective is to minimize the Chamfer loss \mathcal{L}_c and implicit registration cost \mathcal{L}_{sdf} between implicit surface and mesh by filling the gap with the offset Δ estimated from the extra GCN decoder:

$$\mathcal{L}_{\Delta} = \lambda_c \mathcal{L}_c + \lambda_{sdf} \mathcal{L}_{sdf} + \mathcal{L}_{reg} \quad (9)$$

where λ_c is set to 400, and $\lambda_{sdf} = 3$. The Chamfer loss \mathcal{L}_c [5] is defined as below:

$$\mathcal{L}_c = \frac{1}{|\mathcal{M}|} \sum_{V_i \in \mathcal{M}} d(V_i + \Delta_i, \mathcal{M}^*) + \frac{1}{|\mathcal{M}^*|} \sum_{V_j \in \mathcal{M}^*} d(V_j, \mathcal{M})$$

where $d(V_i, \mathcal{M})$ calculates the point to surface distance.

In order to take advantage of pixel-aligned implicit reconstruction, we propose a novel implicit registration loss similar to signed distance function on the offset Δ , which deforms the GCN parametric mesh as close to the shape boundary of the implicit surface reconstructed as possible. Thus, \mathcal{L}_{sdf} is defined as follows:

$$\mathcal{L}_{sdf} = \frac{1}{|\mathcal{M}|} \sum_{V_i \in \mathcal{M}} \|f(\mathcal{F}_{\pi(V_i + \Delta_i)}, V_i + \Delta_i) - \sigma\|_1 \quad (10)$$

where $f(\cdot)$ is the pixel-aligned implicit function defined in Section 3.2, and σ is set to 0.5.

The regularization term \mathcal{L}_{reg} enforces the surface smoothing through minimizing the mesh Laplacian differences and the L_2 norm of offset Δ :

$$\mathcal{L}_{reg} = \lambda_{lap} \|L(V + \Delta) - L(V)\|_2^2 + \lambda_{norm} \|\Delta\|_2^2 \quad (11)$$

where L denotes the Laplacian matrix that retains the mesh regularity. The L_2 norm over mesh offset Δ prevents the vertices from shifting too large. The regularization coefficient λ_{lap} is set to 10^4 , and λ_{norm} is 200.

Implicit Registration Generally, the output of deep neural network produces the coarse prediction, which can be further refined via minimizing the following implicit registration cost:

$$\mathcal{L}_{\mathcal{R}} = \lambda_{sdf} \mathcal{L}_{sdf} + \mathcal{L}_{reg} \quad (12)$$

Since the neural network prediction is close enough to the implicit surface of model-free reconstruction, \mathcal{L}_{sdf} is able to guarantee the convergence. In contrast to training GCN decoder with the loss \mathcal{L}_{Δ} , our proposed implicit registration method does not calculate the point-to-surface Chamfer distance that is very computational insensitive. Therefore, the Chamfer distance calculation is avoided in both inference and refinement stage so that the registration is performed very efficiently in implicit space without extracting the explicit mesh using the marching cube algorithm [16].

4. Experiments

In this section, we give details of our experimental implementation and discuss the results on human reconstruction. We examine the representation capability of our proposed GCN autoencoder for human body. Moreover, we compare the results on both model-based body mesh recovery and model-free reconstruction. In addition, we demonstrate promising results for topology-preserved human reconstruction.

4.1. Experimental Setup

To facilitate the effective experimental evaluation, we conduct the experiments on DeepHuman dataset [35], which contains the total number of 6,795 items, including RGB image, SMPL parameters and meshes reconstructed by a multiview fusion algorithm. We randomly split the samples to form training and testing sets with a ratio of 4 : 1, and obtain 5,436 items for training and 1,439 samples for testing. Due to the privacy issue, the facial regions in image are blurred. Being difficult to recover the thin structures like fingers, the hand geometry of the mesh in the dataset are presented in the form of fists.

In our experiment, we crop the images according to their height and place the human at the center. Then, the cropped image are resized into the resolution of 512×512 . For the model-free implicit surface reconstruction, we convert the meshes in dataset into the watertight one through the robust manifold generation method [9]. Moreover, we transform the resulting mesh into the same coordinates space as the recovered model using GCN decoder by the global pose in dataset. Therefore, the proposed approach is used to fill the gap between the two kinds of reconstruction.

We implemented the proposed approach by PyTorch. The normal estimation network is trained on the DeepHuman training set using Adam optimizer with the learning rate of 2×10^{-4} until convergence. We firstly train the pixel-aligned implicit function and deep feature for the GCN latent space encoder with 60 epochs. Then, the offset decoder is trained and the implicit function is fine-tuned simultaneously for another 10 epochs. We use RMSprop optimizer with the learning rate 10^{-4} that is decayed by the factor of 0.1 at 40-th epoch. We employ 10^4 sampled points to train implicit function, and 7,000 points are used to fine-tune it. In the implicit registration stage, Adam optimizer with learning rate 1×10^{-3} is employed to optimize the mesh vertices offset with 500 iterations.

4.2. Evaluation on Autoencoder

The GCN autoencoder is trained on two motion capture datasets including AMASS [19] and Human3.6M [10] with 10 epochs. AMASS is a large collection of human motion from the marker-based capture system with SMPL representation, and Human3.6M consists of 3.6 million 3D Human poses acquired by recording the performance of 5 female and 6 male subjects. We employ the SMPL model of Human3.6M from [12] to train the GCN autoencoder.

Table 1. Evaluation on autoencoder	
Dataset	MPVAE
AMASS [19]	0.007
Human3.6M [10](train)	0.007
Human3.6M(test)	0.010
DeepHuman [35]	0.010

To effectively optimize the GCN parameters, we use Adam optimizer with the learning rate of 10^{-4} and a weight decay of 10^{-4} . Moreover, the mean per vertex absolute error (MPVAE) is employed as the performance metrics to evaluate the representation capability of different body models. As shown in Table 1, our proposed GCN autoencoder achieves almost the same reconstruction results as the conventional parametric SMPL model. Note that the GCN autoencoder not only has fewer latent parameters but also enjoys the fully convolutional pipeline without involving with the highly nonlinear joint rotation-based mesh generation as SMPL.

4.3. Evaluation on Model-Based Reconstruction

We evaluate the performance of model-based human reconstruction methods on DeepHuman dataset. The hour-glass backbone directly regresses the shape and pose coefficients of SMPL model through a linear layer, which is equivalent to the conventional SMPL model-based human recovery approach [12].



Figure 3. Comparison on model-based reconstruction. We show the results on GCN decoder, GCN decoder without the normal map as input feature, and SMPL coefficients regression.

To facilitate the fair comparison, we employ the same input and backbone network for all the methods, and use the MPVAE and mean per joint position error (MPJPE) as the performance metrics. Table 2 shows the experimental results. It can be clearly seen that our proposed GCN decoder obtains the lower estimation error both on vertices and joints comparing to the SMPL-based method, which demonstrates the effectiveness of the graph convolutional



(a) Input image (b) With normal map (c) Without normal map

Figure 4. Comparison on human reconstruction using pixel-aligned implicit function. We show the results with the normal map as input feature and without the normal map using image only.

network for body mesh representation. Therefore, it is easy to regress the GCN latent embedding than predict the highly nonlinear SMPL coefficients from deep features. Moreover, we evaluate the proposed method using the image only without concatenating the normal map, whose result indicates that the normal map is essential to the accurate reconstruction. Fig. 3 shows the visual results. It can be observed that our proposed GCN decoder is able to capture complex human poses comparing to directly regressing the SMPL coefficients as in [12].

Table 2. Comparison on Model-Based Reconstruction

Methods	MPVAE	MPJPE
SMPL [12]	0.143	72.945
GCN Decoder	0.071	39.994
GCN Decoder w/o normal map	0.089	49.244

4.4. Evaluations on Human Reconstruction

As in [26], we adopt three reconstruction performance metrics including the mean point-to-surface Euclidean distance (P2S), Chamfer distance and normal projection error. P2S and Chamfer distance measure the reconstruction accuracy comparing to the ground-truth mesh. Additionally, the normal projection error is to evaluate the fineness of reconstructed local details as well as the projection consistency.

Table 3 gives the experimental results. It can be seen that our proposed approach performs better than other implicit surface-based methods. Moreover, the normal map can sig-

Table 3. Reconstruction Performance on DeepHuman dataset. * indicates the output mesh has the same topology as SMPL.

Methods	Normal	P2S	Chamfer
PIFu [26]	0.018	0.017	0.016
Ours w only z	0.012	0.025	0.017
Ours w normal	0.009	0.010	0.009
Ours w/o normal	0.015	0.016	0.015
*Inference results	0.037	0.016	0.016
*Refine by Chamfer loss	0.013	0.014	0.012
*Refine by implicit loss	0.016	0.013	0.013



(a) Input image (b) (x, y, z) (c) Only z

Figure 5. Comparison on the input coordinates for the pixel-aligned implicit function. We show the results of full (x, y, z) coordinates and z only.

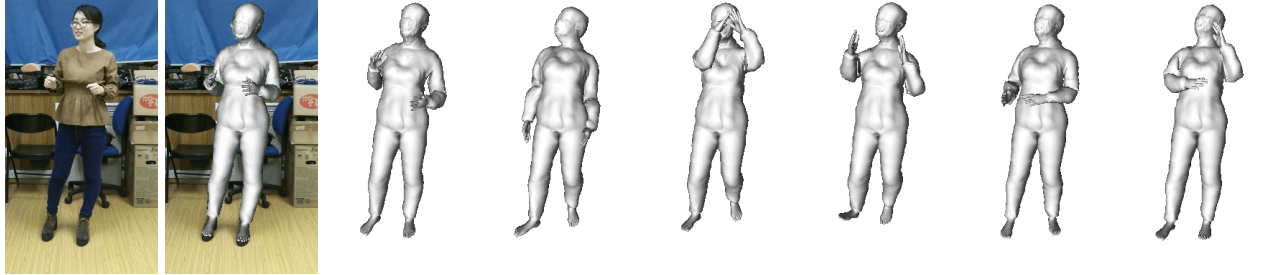
nificantly improve the reconstruction accuracy and capture the clothing details. As shown in Fig. 4, the normal map makes it easier for the implicit function to retain the local details. We evaluate the performance of different coordinate inputs on calculating the implicit occupancy function. As shown in Fig. 10, the implicit function with full (x, y, z) coordinates obtains more accurate results than the one only using z coordinate [26] that can not generalize well on recovering body parts like hands and feet.

We compare our proposed topology-preserved reconstruction approach against the conventional Chamfer distance-based registration method used in IPNet [4]. As shown in Table 3, the network inference predicts the coarse mesh, which can be effectively refined by our proposed implicit registration. Fig. 6 shows the comparison results. It can be seen that the presented method performs comparable with conventional Chamfer distance-based method. By tak-



(a) Input image (b) Inference (c) Implicit loss (d) Chamfer loss (e) Input image (f) Inference (g) Implicit loss (h) Chamfer loss

Figure 6. Comparison on the human reconstruction. We show the results of network inference (b,f), our proposed implicit registration (c,g) and conventional Chamfer loss (d,h), respectively.



(a) Input image (b) Recovered (c) Reposed (d) Reposed (e) Reposed (f) Reposed (g) Reposed (h) Reposed

Figure 7. Visual results of reposing the recovered mesh

ing advantage of the fixed topology, we can easily animate the recovered mesh in arbitrary poses, as shown in Fig. 12.

As depicted in Table 4, the optimization time for our approach is about seven times faster than the Chamfer distance-based method. This is because the proposed implicit distance is efficient to compute comparing to Chamfer loss that needs to search for the nearest neighbors. The forward inference time of the proposed network is 0.11s. Our method does not require to extract the mesh by marching cube [16], which saves the extra computational time.

Table 4. Comparison on Computational Time

Methods	Marching Cube	Optimization	Total
Chamfer Registration	7.3s	42.4s	49.7s
Ours	-	5.9s	5.9s

5. Conclusions

This paper proposed a novel topology-preserved human reconstruction approach to bridging the gap between

model-based and model-free human reconstruction. The presented end-to-end neural network simultaneously predicts the pixel-aligned implicit surface and the explicit mesh surface built by graph convolutional neural network. Moreover, we propose the extra graph convolutional neural network to estimate the vertex offsets between the implicit surface and parametric mesh model. Furthermore, we suggest the efficient implicit registration method to refine the neural network output in implicit space. We have conducted the evaluation on DeepHuman dataset. The encouraging experimental results showed that our proposed approach is able to effectively recover the accurate mesh model while preserving the topology.

Despite these promising results, some limitations and future directions should be addressed. Our current experiments rely on the dataset that treats the imperfect reconstruction results as ground-truth. The blurred facial region leads to the flat mesh in head. In future, we will address these issues by building more accurate human models for

training.

References

- [1] Thiemo Alldieck, Marcus A. Magnor, Bharat Lal Bhatnagar, Christian Theobalt, and Gerard Pons-Moll. Learning to reconstruct people in clothing from a single RGB camera. In *CVPR*, pages 1175–1186. Computer Vision Foundation / IEEE, 2019.
- [2] Thiemo Alldieck, Marcus A. Magnor, Weipeng Xu, Christian Theobalt, and Gerard Pons-Moll. Detailed human avatars from monocular video. In *3DV*, pages 98–109. IEEE Computer Society, 2018.
- [3] Dragomir Anguelov, Praveen Srinivasan, Daphne Koller, Sebastian Thrun, Jim Rodgers, and James Davis. SCAPE: shape completion and animation of people. *ACM Trans. Graph.*, 24(3):408–416, 2005.
- [4] Bharat Lal Bhatnagar, Cristian Sminchisescu, Christian Theobalt, and Gerard Pons-Moll. Combining implicit function learning and parametric models for 3d human reconstruction. In *ECCV (2)*, volume 12347 of *Lecture Notes in Computer Science*, pages 311–329. Springer, 2020.
- [5] Bharat Lal Bhatnagar, Cristian Sminchisescu, Christian Theobalt, and Gerard Pons-Moll. Combining implicit function learning and parametric models for 3d human reconstruction. In *European Conference on Computer Vision (ECCV)*. Springer, aug 2020.
- [6] Federica Bogo, Angjoo Kanazawa, Christoph Lassner, Peter V. Gehler, Javier Romero, and Michael J. Black. Keep it SMPL: automatic estimation of 3d human pose and shape from a single image. In *ECCV (5)*, volume 9909 of *Lecture Notes in Computer Science*, pages 561–578. Springer, 2016.
- [7] Hongsuk Choi, Gyeongsik Moon, and Kyoung Mu Lee. Pose2mesh: Graph convolutional network for 3d human pose and mesh recovery from a 2d human pose. In *ECCV (7)*, volume 12352 of *Lecture Notes in Computer Science*, pages 769–787. Springer, 2020.
- [8] Valentin Gabeur, Jean-Sébastien Franco, Xavier Martin, Cordelia Schmid, and Grégory Rogez. Moulding humans: Non-parametric 3d human shape estimation from single images. In *ICCV*, pages 2232–2241. IEEE, 2019.
- [9] Jingwei Huang, Hao Su, and Leonidas J. Guibas. Robust watertight manifold surface generation method for shapenet models. *CoRR*, abs/1802.01698, 2018.
- [10] Catalin Ionescu, Dragos Papava, Vlad Olaru, and Cristian Sminchisescu. Human3.6m: Large scale datasets and predictive methods for 3d human sensing in natural environments. *IEEE Trans. Pattern Anal. Mach. Intell.*, 36(7):1325–1339, 2014.
- [11] Hanbyul Joo, Tomas Simon, and Yaser Sheikh. Total capture: A 3d deformation model for tracking faces, hands, and bodies. In *CVPR*, pages 8320–8329. IEEE Computer Society, 2018.
- [12] Angjoo Kanazawa, Michael J. Black, David W. Jacobs, and Jitendra Malik. End-to-end recovery of human shape and pose. In *CVPR*, pages 7122–7131. IEEE Computer Society, 2018.
- [13] Nikos Kolotouros, Georgios Pavlakos, Michael J. Black, and Kostas Daniilidis. Learning to reconstruct 3d human pose and shape via model-fitting in the loop. In *ICCV*, pages 2252–2261. IEEE, 2019.
- [14] Zorah Löhner, Daniel Cremers, and Tony Tung. Deepwrinkles: Accurate and realistic clothing modeling. In *ECCV (4)*, volume 11208 of *Lecture Notes in Computer Science*, pages 698–715. Springer, 2018.
- [15] Matthew Loper, Naureen Mahmood, Javier Romero, Gerard Pons-Moll, and Michael J. Black. SMPL: a skinned multi-person linear model. *ACM Trans. Graph.*, 34(6):248:1–248:16, 2015.
- [16] William E. Lorensen and Harvey E. Cline. Marching cubes: A high resolution 3d surface construction algorithm. In *SIGGRAPH*, pages 163–169. ACM, 1987.
- [17] Qianli Ma, Jinlong Yang, Anurag Ranjan, Sergi Pujades, Gerard Pons-Moll, Siyu Tang, and Michael J. Black. Learning to dress 3d people in generative clothing. In *CVPR*, pages 6468–6477. IEEE, 2020.
- [18] Andrew L Maas, Awni Y Hannun, and Andrew Y Ng. Rectifier nonlinearities improve neural network acoustic models. In *Proc. icml*, volume 30, page 3. Citeseer, 2013.
- [19] Naureen Mahmood, Nima Ghorbani, Nikolaus F. Troje, Gerard Pons-Moll, and Michael J. Black. AMASS: Archive of motion capture as surface shapes. In *International Conference on Computer Vision*, pages 5442–5451, Oct. 2019.
- [20] Ryota Natsume, Shunsuke Saito, Zeng Huang, Weikai Chen, Chongyang Ma, Hao Li, and Shigeo Morishima. Siclope: Silhouette-based clothed people. In *CVPR*, pages 4480–4490. Computer Vision Foundation / IEEE, 2019.
- [21] Alexandros Neophytou and Adrian Hilton. A layered model of human body and garment deformation. In *3DV*, pages 171–178. IEEE Computer Society, 2014.
- [22] Alejandro Newell, Kaiyu Yang, and Jia Deng. Stacked hourglass networks for human pose estimation. In *ECCV (8)*, volume 9912 of *Lecture Notes in Computer Science*, pages 483–499. Springer, 2016.
- [23] Georgios Pavlakos, Vasileios Choutas, Nima Ghorbani, Timo Bolkart, Ahmed A. A. Osman, Dimitrios Tzionas, and Michael J. Black. Expressive body capture: 3d hands, face, and body from a single image. In *CVPR*, pages 10975–10985. Computer Vision Foundation / IEEE, 2019.
- [24] Gerard Pons-Moll, Sergi Pujades, Sonny Hu, and Michael J. Black. Clothcap: seamless 4d clothing capture and retargeting. *ACM Trans. Graph.*, 36(4):73:1–73:15, 2017.
- [25] Anurag Ranjan, Timo Bolkart, Soubhik Sanyal, and Michael J. Black. Generating 3d faces using convolutional mesh autoencoders. In *ECCV (3)*, volume 11207 of *Lecture Notes in Computer Science*, pages 725–741. Springer, 2018.
- [26] Shunsuke Saito, Zeng Huang, Ryota Natsume, Shigeo Morishima, Hao Li, and Angjoo Kanazawa. Pifu: Pixel-aligned implicit function for high-resolution clothed human digitization. In *ICCV*, pages 2304–2314. IEEE, 2019.
- [27] Shunsuke Saito, Tomas Simon, Jason M. Saragih, and Hanbyul Joo. Pifuhd: Multi-level pixel-aligned implicit function for high-resolution 3d human digitization. In *CVPR*, pages 81–90. IEEE, 2020.

- [28] Sicong Tang, Feitong Tan, Kelvin Cheng, Zhaoyang Li, Siyu Zhu, and Ping Tan. A neural network for detailed human depth estimation from a single image. In *ICCV*, pages 7749–7758. IEEE, 2019.
- [29] Gül Varol, Duygu Ceylan, Bryan C. Russell, Jimei Yang, Ersin Yumer, Ivan Laptev, and Cordelia Schmid. Bodynet: Volumetric inference of 3d human body shapes. In *ECCV (7)*, volume 11211 of *Lecture Notes in Computer Science*, pages 20–38. Springer, 2018.
- [30] Ting-Chun Wang, Ming-Yu Liu, Jun-Yan Zhu, Andrew Tao, Jan Kautz, and Bryan Catanzaro. High-resolution image synthesis and semantic manipulation with conditional gans. In *CVPR*, pages 8798–8807. IEEE Computer Society, 2018.
- [31] Yuxin Wu and Kaiming He. Group normalization. In *ECCV (13)*, volume 11217 of *Lecture Notes in Computer Science*, pages 3–19. Springer, 2018.
- [32] Donglai Xiang, Hanbyul Joo, and Yaser Sheikh. Monocular total capture: Posing face, body, and hands in the wild. In *CVPR*, pages 10965–10974. Computer Vision Foundation / IEEE, 2019.
- [33] Jinlong Yang, Jean-Sébastien Franco, Franck Hétroy-Wheeler, and Stefanie Wuhler. Analyzing clothing layer deformation statistics of 3d human motions. In *ECCV (7)*, volume 11211 of *Lecture Notes in Computer Science*, pages 245–261. Springer, 2018.
- [34] Tao Yu, Zerong Zheng, Kaiwen Guo, Jianhui Zhao, Qionghai Dai, Hao Li, Gerard Pons-Moll, and Yebin Liu. Doublefusion: Real-time capture of human performances with inner body shapes from a single depth sensor. In *CVPR*, pages 7287–7296. IEEE Computer Society, 2018.
- [35] Zerong Zheng, Tao Yu, Yixuan Wei, Qionghai Dai, and Yebin Liu. Deephuman: 3d human reconstruction from a single image. In *ICCV*, pages 7738–7748. IEEE, 2019.
- [36] Hao Zhu, Xinxin Zuo, Sen Wang, Xun Cao, and Ruigang Yang. Detailed human shape estimation from a single image by hierarchical mesh deformation. In *CVPR*, pages 4491–4500. Computer Vision Foundation / IEEE, 2019.

A. GCN Network Architecture

Table 5. Encoder architecture

Layer	Input size	Output size
ConvResBlock 1	6890×3	6890×64
ConvResBlock 2	6890×64	3445×64
ConvResBlock 3	3445×64	3445×128
ConvResBlock 4	3445×128	1723×128
ConvResBlock 5	1723×128	1723×256
ConvResBlock 6	1723×256	862×256
ConvResBlock 7	862×256	862×512
ConvResBlock 8	862×512	862×512
Chebyshev Conv	862×512	862×64
Fully Connected	862×64	64

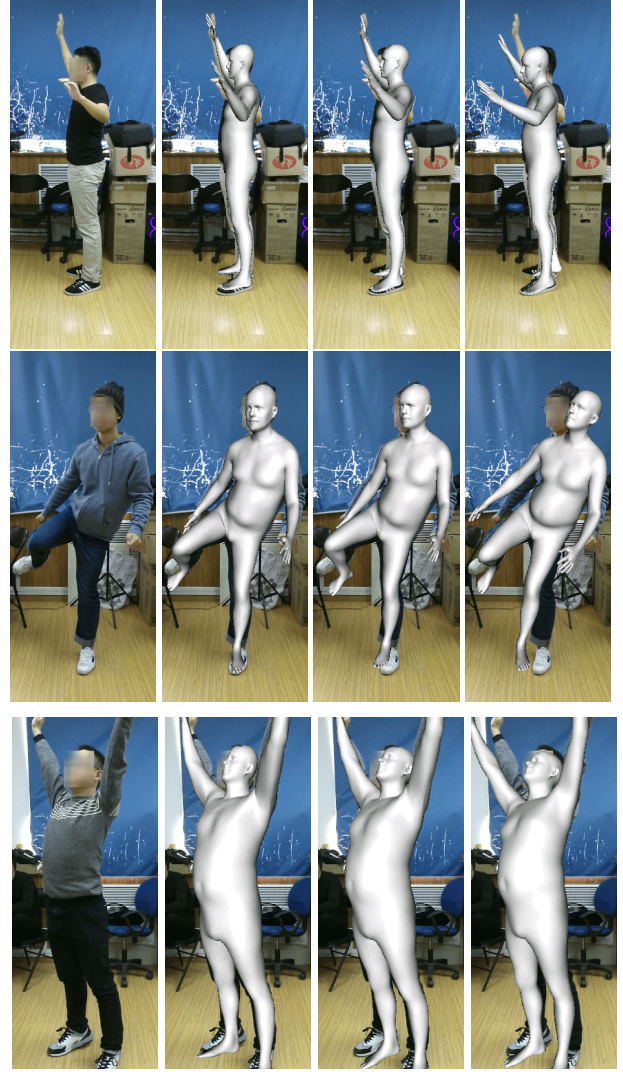
Table 5 and Table 6 show our detailed architecture of the GCN autoencoder. the encoder is made of eight Chebyshev Residual Blocks with Chebyshev polynomial of order two, a Chebyshev convolution with order one and a fully connected layer. Each graph convolution layer is followed by a Leaky ReLU. The architecture of decoder is similar to the encoder except having the group normalization before Leaky ReLU.

B. More Visual Results

In this section, we propose more visual results of our method. Fig. 8 shows more results about the representation ability of our GCN autoencoder. Fig. 9 provides more visual results about failure cases which use only z coordinate. Fig. 11 gives more visual results about the comparison between our proposed implicit registration and conventional Chamfer distance-based registration method. Fig. 12 shows the results of animating the reconstructed textured mesh. The color of each vertex is sampled from the original image.

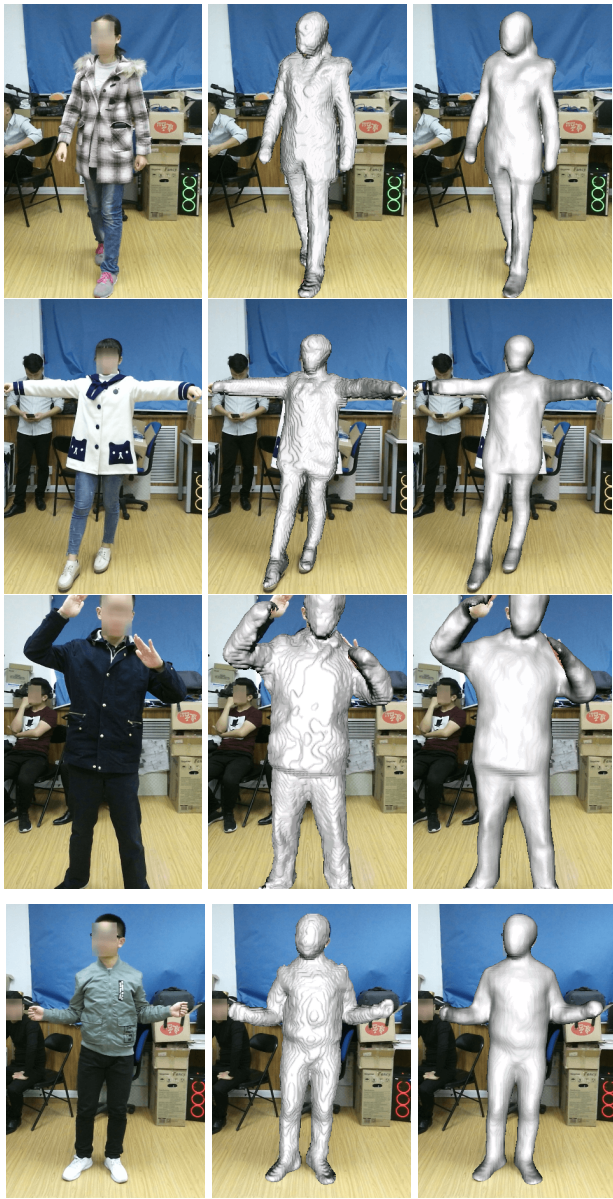
Table 6. Decoder architecture

Layer	Input size	Output size
Fully Connected	64	862×64
Chebyshev Conv	862×64	862×512
DConvResBlock 1	862×512	862×512
DConvResBlock 2	862×512	862×256
DConvResBlock 3	862×256	1723×256
DConvResBlock 4	1723×256	1723×128
DConvResBlock 5	1723×128	3445×128
DConvResBlock 6	3445×128	3445×64
DConvResBlock 7	3445×64	6890×64
DConvResBlock 8	6890×64	6890×3



(a) Input image (b) GCN (c) w/o normal (d) SMPL

Figure 8. Comparison on model-based reconstruction. We show the results on GCN decoder, GCN decoder without the normal map as input feature, and SMPL coefficients regression.



(a) Input image (b) With normal map (c) Without normal map

Figure 9. Comparison on human reconstruction using pixel-aligned implicit function. We show the results with the normal map as input feature and without the normal map using image only.



(a) Input image (b) (x, y, z) (c) Only z

Figure 10. Comparison on the input coordinates for the pixel-aligned implicit function. We show the results of full (x, y, z) coordinates and z only.



(a) Input image (b) Inference (c) Implicit loss (d) Chamfer loss (e) Input image (f) Inference (g) Implicit loss (h) Chamfer loss

Figure 11. Comparison on the human reconstruction. We show the results of network inference (b,f), our proposed implicit registration (c,g) and conventional Chamfer loss (d,h), respectively.



(a) Input image (b) Recovered (c) Reposed (d) Reposed (e) Reposed (f) Reposed (g) Reposed (h) Reposed

Figure 12. Visual results of textured reposing the recovered mesh